Strong kinetics-stress coupling in lithiation of Si and Ge anodes

Hui Yang [a], Wentao Liang [a], Xu Guo [b], Chong-Min Wang [c], Sulin Zhang [a],*

[a] Department of Engineering Science and Mechanics, Pennsylvania State University, University Park, PA 16802, United States
[b] Department of Engineering Mechanics, Dalian University of Technology, Dalian, 116023, PR China
[c] Environmental Molecular Sciences Laboratory, Pacific Northwest National Laboratory, 902 Battelle Boulevard, Richland, WA 99352, United States

ARTICLE INFO

ABSTRACT

Coupling between transport kinetics of chemical participants and mechanical stress is a universal phenomenon in numerous chemo-physical processes. In this Letter, we present a set of *in-situ* transmission electron microscopy studies along with atomistically informed continuum mechanics modeling to evidence the strong coupling between lithiation kinetics and stress generation and failure of silicon (Si) and germanium (Ge) electrodes. On the one hand, we show that anisotropic lithiation in crystalline Si (c-Si) leads to anisotropic swelling and surface fracture, in contrast to isotropic lithiation, isotropic swelling, and tough behavior in c-Ge and amorphous Si (a-Si). On the other, we demonstrate that lithiation self-generated stress leads to lithiation retardation and externally applied bending breaking the lithiation symmetry in c-Ge nanowires. Our studies shed lights on the design of durable high-performance lithium ion batteries.

© 2014 Elsevier Ltd. All rights reserved.

Mechanics plays a key role in numerous bio-chemo-physical processes, ranging from stress-mediated chemical reactions and mass diffusion [1–3], to force-modulated biochemical signaling [4]. Reciprocally, local chemical environment and the associated kinetics may also mediate stress generation and mechanical failure of the materials, as exemplified by the hydrogen and lithium (Li) embrittlement [5,6], oxygen-regulated fracture paths in graphene [7], and stress fiber formation in living cells [8]. Such kinetics-stress coupling is universal, but particularly predominant in the electrochemical lithiation of the high-capacity electrode materials, including silicon (Si) and germanium (Ge). Understanding the bidirectional coupling effect is imperative for defining the driving forces for these processes in general and mitigating the chemomechanical failure of the high capacity electrode materials in particular.

Herein we present a set of *in-situ* transmission electron microscopy (TEM) studies corroborated with atomistically informed continuum mechanics modeling on single nanoparticle or single nanowire level to elucidate the coupling between the lithiation kinetics and stress generation and failure of Si and Ge. The *in-situ* TEM study is enabled by the electrochemical platform with a half-cell nanobattery as the key component. The nanobattery consists of single nanowires or single nanoparticles as the working electrode, lithium (Li) metal as the counter electrode, and the natively grown lithium oxide (Li_2O) on the Li metal surface as the solid electrolyte [9,10]. The nanobattery can be cyclically lithiated and delithiated inside a TEM, which allows real-time imaging of phase transformation, morphological change, and fracture of the nanosale electrodes [6,11–16].

The continuum mechanics model couples Li transport kinetics with large elasto-plasticity to account for the lithiation-induced volumetric change and stress [17,18]. In particular, Li insertion induces chemical strain
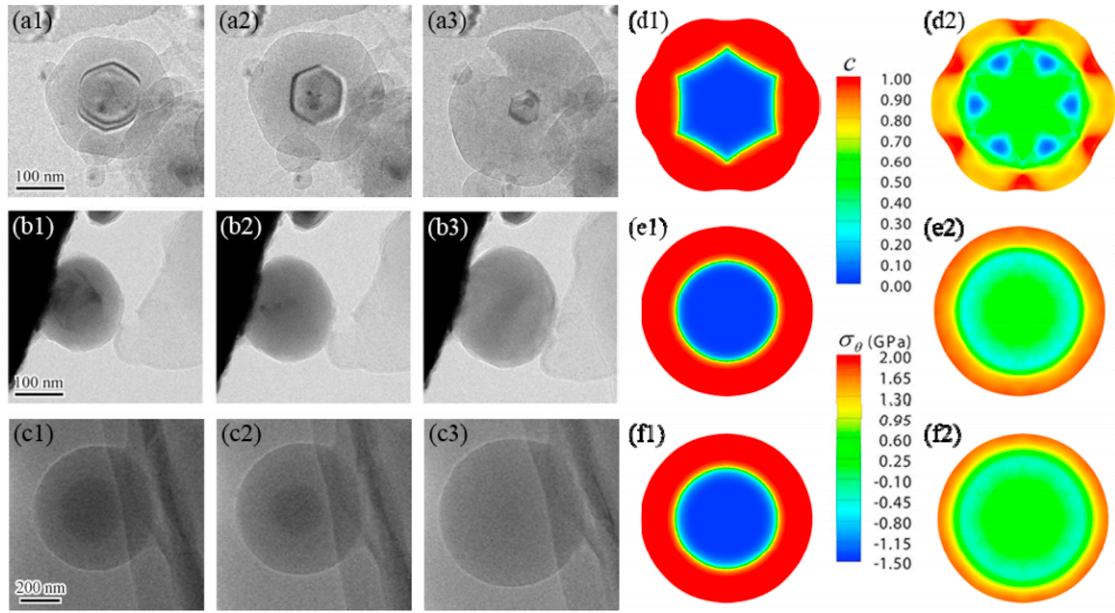
Fig. 1. **Left**: Lithiation-induced anisotropic swelling and fracture in a *c*-SiNP versus the isotropic swelling without fracture in a *c*-GeNP (Adapted with permission from ref. [16]. © 2013, American Chemical Society) and *a*-SiNP (Adapted with permission from ref. [29]. © 2013, American Chemical Society). The original sizes of both *c*-Si and *c*-Ge NPs are about 160 nm, and *a*-SiNP is about 540 nm. (a1) Partially lithiated *c*-SiNP showing the hexagon-shaped *c*-Si core with the {110} facets. (a2, a3) Fracture occurred in a late stage of lithiation. (b1, b2) Partially lithiated *c*-GeNP showing the rounded *c*-Ge core. (b3) Full lithiation without fracture of a *c*-GeNP. (c1, c2) Partially lithiated *a*-SiNP showing the rounded *a*-Si core. (c3) Full lithiation without fracture of an *a*-SiNP. **Right**: Chemo-mechanical modeling of the core–shell structure and stress generation in the cross section of a lithiated nanowire, showing the effect of the lithiation anisotropy. (d1) Orientation-dependent interfacial reaction rate in ⟨111⟩-oriented *c*-SiNW leads to a hexagonal shaped reaction front in the cross section of the nanowire, represented by the transition colors from red to blue. (e1, f1) Isotropic interfacial reaction rate results in circular shaped reaction fronts in the cross sections of *c*-GeNW and *a*-SiNW. (d1, e1, f1) Li concentration *c* is normalized by that of the corresponding fully lithiated product $Li_{3.75}M$ (M = Si or Ge). (d2, e2, f2) Hoop stress (σ_θ) profiles in cross sections of ⟨111⟩ *c*-Si (d2), *c*-Ge (e2) and *a*-Si (f2) nanowires. Lithiation anisotropy causes the intensified hoop tension at the angular sites between two {110} adjacent facets in the ⟨111⟩-oriented *c*-SiNW (d2), while such intensified tension is absent in the other two nanowires (e2 and f2).

that adds to the elasto-plastic strain in the general finite-deformation kinematics [18–22]. In turn, the local stress state alters the chemical potential of Li, and hence its transport kinetics [23,24]. Lithiation involves two concurrent processes in series: reaction at the reaction front and Li diffusion behind it [14]. Despite the difference in the physical processes of interfacial reaction and bulk diffusion, we here simulate the two concurrent processes, i.e., reaction and diffusion, in a unified manner by treating the interfacial reaction as non-linear diffusion across a diffuse interfacial domain for numerical convenience [17,18,22]. To incorporate the stress effect on Li transport, both the reaction rate at the reaction front and the Li diffusivity in the lithiated region are set to be stress dependent, e.g.,

$$D_{eff} = D_{sf}(c)\exp(\sigma_h\Omega/k_BT) \tag{1}$$

where Ω is the activation volume of Li diffusion, k_BT is the thermal energy, and σ_h is the hydrostatic stress [25–28]. The Li diffusivity in the stress-free condition D_{sf} is generally set to be a function of Li concentration *c*. An appropriately chosen function form of $D_{sf}(c)$ can capture the non-linear diffusion and define a sharp or diffusive interface between the lithiated and unlithiated regions [13,17, 18,22]. From the stress-dependent exponential term, tensile stress enhances reaction and diffusion, while compressive stress suppresses them.

Lithiation kinetics modulates stress generation and fracture. Previous studies revealed several features in

lithiation shared by crystalline Si (*c*-Si) and Ge (*c*-Ge). Owing to the much higher surface diffusivity than the bulk in Si and Ge, Li quickly covers the surface of the nanostructures, and then flows inward, forming a core–shell structure with lithiated amorphous outer shell and unlithiated crystalline inner core [13,15,16,28,30]. As lithiation proceeds, the shell thickens and the core shrinks. The amorphous-crystalline interface (ACI) separating the shell and the core was revealed to be atomically sharp [14,16, 29,30], with a width of only ~1 nm [14,31,32]. Across the interface, the Li concentration drops abruptly from $Li_{3.75}M$ (M = Si or Ge) to *c*-M. The amorphous region undergoes very large volume increase (~300% for *c*-Si [13] and ~260% for *c*-Ge [16,28]) due to Li insertion. Large incompatible strain and stress are generated at the reaction front, i.e., the ACI. Owing to the constraint of the stiff unlithiated crystalline core, newly lithiated product ($Li_{3.75}M$) during lithiation is pushed outward in the direction normal to the reaction front. The pushing-out effect generates large hoop tension (σ_θ) in the amorphous outer shell that may lead to initiation of fracture [16,18]. For amorphous Si (*a*-Si), lithiation proceeds in a two-step manner: *a*-Si first undergoes a phase transition to $a\text{-}Li_{2.5}Si$, followed by a second-step lithiation to $a\text{-}Li_{3.75}Si$. Despite this difference, lithiation of *a*-Si also features the core–shell structure and the sharp interface in the first step [29,33].

A key distinction in the lithiation of *c*-Si, *a*-Si, and *c*-Ge is that lithiation proceeds isotropically in *c*-Ge and
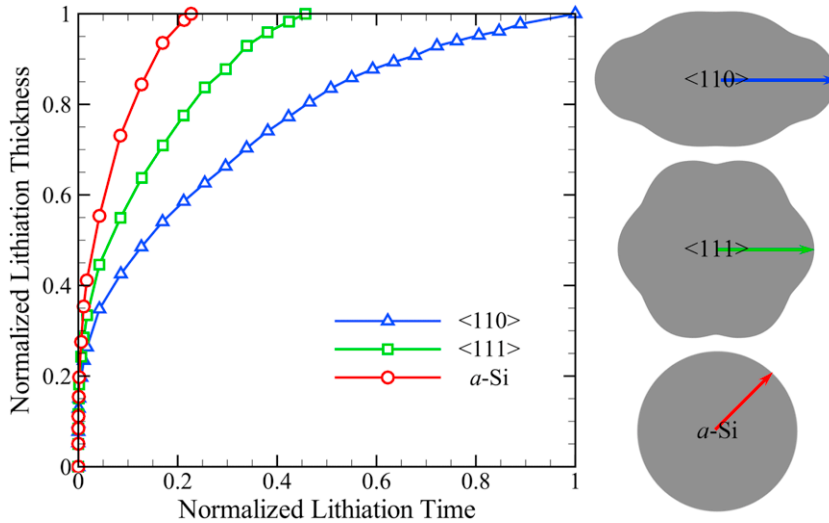
Fig. 2. Thickness evolution of the fully lithiated a-Li$_x$Si shell in the cross sections of $\langle 110 \rangle$- and $\langle 111 \rangle$-oriented c-SiNWs and of an a-SiNW. The lithiation thickness is measured in the deformed configuration and normalized by the thickness of fully lithiated SiNWs, while the lithiation time is normalized by that required for fully lithiating the $\langle 110 \rangle$-oriented c-SiNW. For c-SiNWs the fully lithiated thickness is measured in the {110} direction, while for a-SiNW in an arbitrary direction because of its isotropic lithiation.

a-Si [16,29,30,33], but anisotropically in c-Si [13,34,35]. As shown in Figs. 1(a1–a3), the partially lithiated c-Si nanoparticle (c-SiNP) exhibited a hexagonal profile in the projected plane, both for the outer surface and the ACI, suggesting lithiation anisotropy. The surviving facets constituting the inner surface (the ACI) are likely {110} surfaces as the lithiation rate along $\langle 110 \rangle$ direction is much higher than any other directions. In contrast, lithiation of c-GeNP (Figs. 1(b1–b3)) and a-SiNP (Figs. 1(c1–c3)) causes uniform expansion along all the directions, manifested by nearly unchanged shapes of the nanoparticles during lithiation, demonstrating lithiation isotropy.

The difference in the lithiation kinetics results in apparent differences in the stress generation and fracture behavior. For anisotropic lithiation in c-Si, since the {110} facets are lithiated much faster, much stronger pushing-out effect is generated along the $\langle 110 \rangle$ directions than any other directions, leading to large non-uniform hoop tension at the outer lithiated shell. In particular, hoop tension (σ_θ) at the angular sites between two adjacent {110} facets is significantly intensified (Figs. 1(d1–d2)) in a $\langle 111 \rangle$-oriented crystalline silicon nanowire (c-SiNW), as large incompatible strain is developed as a result of the anisotropic pushing-out effect. These angular sites are identified as the spots of the onset of fracture, consistent with the TEM observation shown in Fig. 1(a3). While for isotropic lithiation of c-GeNW and a-SiNW, the uniform pushing-out effect results in isotropic lithiation morphologies (Figs. 1(e1–e2) for c-GeNW and Figs. 1(f1–f2) for a-SiNW). The resulting hoop tension in the outer shell is also uniform. The lack of stress-intensified sites on the outer shell inhibits the initiation of fracture in lithiated c-GeNW and a-SiNW. Our previous *in-situ* TEM studies showed that c-GeNPs remain tough upon cyclic lithiation and delithiation [16]. In simulating the two-step lithiation in a-Si, we first partially lithiate the nanowire to a-Li$_{2.5}$Si, and then to a-Li$_{3.75}$Si. The first-step lithiation results in a sharp interface, while the second a diffuse interface. Figs. 1(f1–f2)

plot the Li concentration and stress distribution at the state when the two reaction fronts coincide, which represents the most critical condition but experimentally may not be realistic. The stress profile clearly shows that the two-step lithiation alleviates the abruptness of the interface and hence the incompatible stress at the interface. The pushing-out effect is also weaker, and hence reduced hoop tension in the outer shell, as compared to the lithiation generated stress in the c-GeNW (Figs. 1(e1–e2)). This explains the tough behavior of micron-sized a-Si during lithiation in previous studies [29,36].

Mechanical stress mediates lithiation kinetics. Li insertion generates compressive stress both at and closely behind the reaction front in the electrodes [18]. The compressive stress suppresses Li reaction at the reaction front as well as Li diffusion behind it, thus slowing down further lithiation. Such stress-induced lithiation retardation has been demonstrated by recent *in-situ* TEM studies: the migration of the lithiation reaction front in both Si and Ge slowed down considerably as lithiation proceeded [26,28,37]. The lithiation-induced compressive stress in Si could be high enough to completely override the electrochemical driving forces on reaction and diffusion, leading to the stagnation of lithiation. Thus, lithiation-induced stresses play an important role in the kinetics of Li insertion and extraction in electrodes, which will subsequently affect the charging and discharging rates.

Lithiation anisotropy influences the distribution and level of stress near the ACI, which in turn mediates the lithiation rate. Fig. 2 shows the simulated time evolution of the lithiation depth in the cross sections of an a-SiNW and $\langle 110 \rangle$- and $\langle 111 \rangle$-oriented c-SiNWs. The lithiation depth is measured in the lithiated configuration and normalized by the thickness of the fully lithiated SiNWs. For c-SiNWs the fully lithiated thickness is measured in the {110} direction, while for the a-SiNW in an arbitrary radial direction, as marked by the colored arrows in the deformed
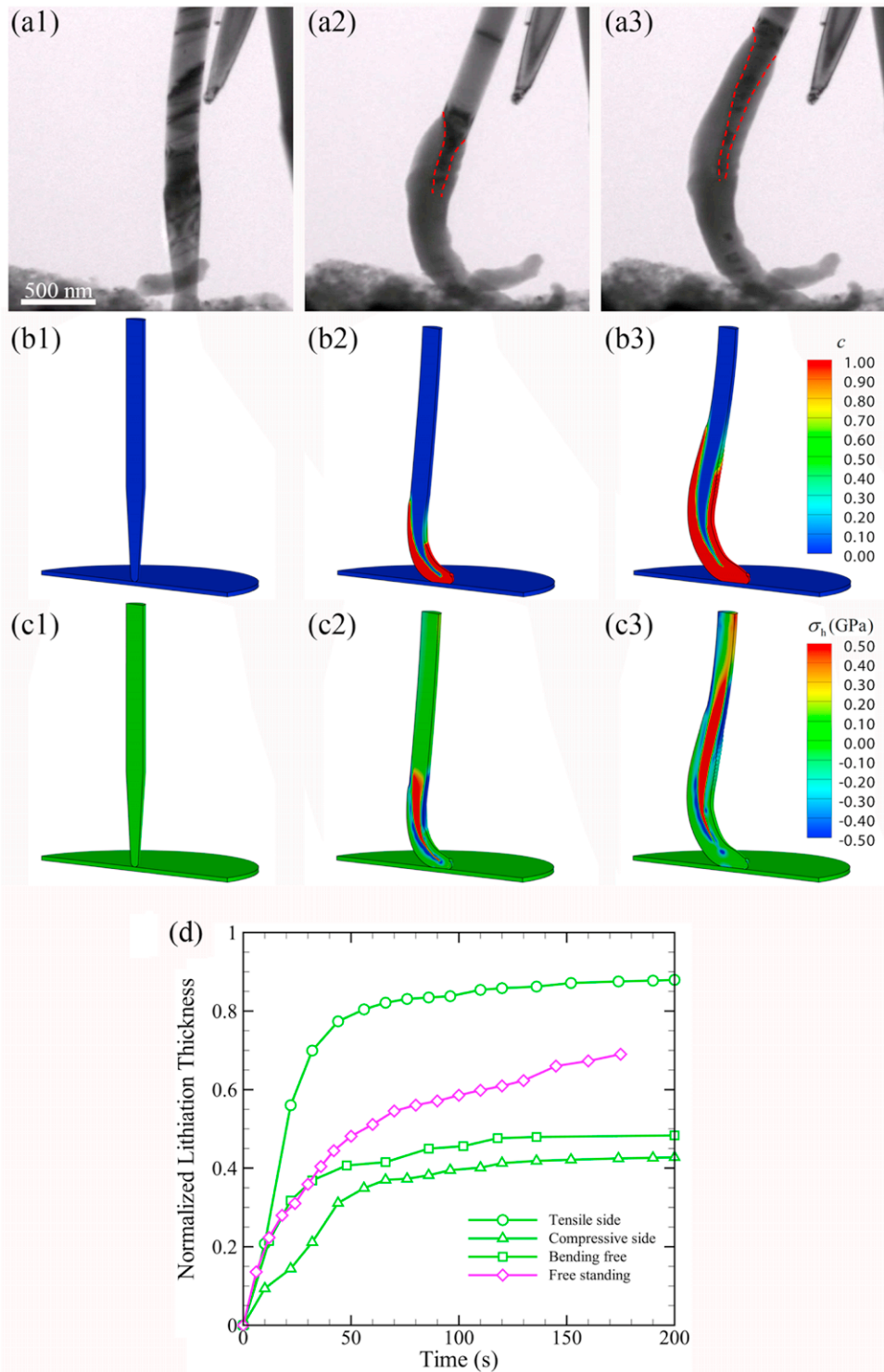
Fig. 3. (a1–a3): TEM snapshots showing the symmetry-breaking in lithiation of a bent GeNW. The GeNW was pushed against the Li metal to create bending during the lithiation processes, leading to lithiation asymmetry. The unlithiated crystalline core in the GeNW is outlined by the dashed red lines. (b1–b3): 3D chemo-mechanical modeling of Li concentration profiles at different lithiation stages in a GeNW subject to bending. Symmetry breaking of lithiation is clearly shown by the Li distribution on the symmetric plane in the longitudinal direction. (c1–c3): Corresponding simulated hydrostatic stress distributions of the bent GeNW. (d): Lithiation kinetics of the GeNWs measured from *in-situ* TEM imaging (Adapted with permission from ref. [28]. © 2014, American Chemical Society). The comparison of lithiation kinetics between bent and free-standing GeNW demonstrates the symmetry-breaking of lithiation by bending.

cross sections of the SiNWs in Fig. 2. The lithiation times for all the cases are normalized by that required for fully lithiating the $\langle 110 \rangle$-oriented c-SiNW. The slopes of these curves indicate the lithiation rates. At the early stage of lithiation, the lithiation depths of all SiNWs evolve nearly at the same high rate, corresponding to the fast surface lithiation of the nanowires. With the inward movement of the reaction front in the radial direction, lithiation-induced hydrostatic compression retards further lithiation. As lithiation progresses the compressive stress at and near the ACI also increases, leading to an increasingly pronounced retardation effect. Our simulations clearly show that with increasing lithiation anisotropy (a-SiNW $< \langle 111 \rangle$ c-SiNW $< \langle 110 \rangle$ c-SiNW [17]) the retardation effect is increasingly pronounced.

Similar to the lithiation self-generated stress, externally applied load may also mediate lithiation kinetics [28]. In particular, bending of a nanowire can generate asymmetric stress profile, and could potentially bias the lithiation rate. We characterized in situ the lithiation kinetics of c-GeNWs under bending and compared to a free-standing c-GeNW. Figs. 3(a1–a3) show the lithiation kinetics of a c-GeNW under bending. The c-GeNW was pushed sideways to the left, creating a bending force in the nanowire. At the highly bent region, the nanowire underwent tension on the left side and compression on the right. Correspondingly, lithiation proceeded markedly faster on the tensile side than the compressive side, breaking lithiation symmetry in free-standing nanowires. Figs. 3(b1–b3) and (c1–c3) plot the longitudinal cross-sectional view of the Li concentration profiles and stress distributions at three different lithiation snapshots simulated by the continuum model, respectively. Both agree with the *in-situ* TEM imaging.

Fig. 3(d) plots the time-dependent thickness of the lithiation shell for a bent GeNW and a free-standing GeNW. The thickness is normalized by the diameter of the corresponding pristine GeNWs. For the free-standing GeNW, lithiation slowed down as lithiation proceeded, exhibiting self-regulated lithiation retardation, similar to the SiNWs shown in Fig. 2. For the bent GeNW, we chose two representative cross-sections in the axial direction, one located at the highly curved point, and the other at the straight portion of the GeNW. In order to capture the symmetry breaking at the curved segment, we plot the lithiated thicknesses of the tensile and compressive sides separately. From all the three curves associated with the bent GeNW, lithiation started with a very high rate, and slowed down gradually. The initial lithiation rate for the tensile side of the cross-section of the bent point is the highest, manifested by the steepest slope of the curve. The data points for the straight point (bending-free) completely fell between those for the tensile and compressive sides, indicating an intermediate stress state of this cross-section. We note that the curve for the straight point is closer to that for the compressive side of the curved cross-section, indicating an asymmetric dependence of the lithiation rate on the compression and tension. Furthermore, after a fast lithiation regime, the lithiation kinetics curves for all the three cross-sections become flat, indicating that lithiation came to a nearly complete stop.

Correspondingly, very high compressive stress must be generated in all the cross sections. By comparison, lithiation retardation in the bent GeNW is apparently stronger than that of the free-standing GeNW since the pushing force also generated considerable axial compression in the bent GeNW.

In conclusion, the *in-situ* TEM experiments and modeling results provided here demonstrate the strong coupling between lithiation kinetics and the degradation of Si and Ge-based electrodes. Our understanding of the coupling effect may shed light on the design of durable high-capacity electrodes, by either electrochemically controlling the lithiation kinetics or mechanically manipulating the stress generation.

References

[1] F.C. Larcht'e, J.l. Cahn, The effect of self-stress on diffusion in solids, Acta Metall. 30 (10) (1982) 1835–1845.

[2] T. Garnier, V.R. Manga, D.R. Trinkle, M. Nastar, P. Bellon, Stress-induced anisotropic diffusion in alloys: complex Si solute flow near a dislocation core in Ni, Phys. Rev. B 88 (13) (2013) 134108.

[3] M.M. Caruso, D.A. Davis, Q. Shen, S.A. Odom, N.R. Sottos, S.R. White, J.S. Moore, Mechanically-induced chemical changes in polymeric materials, Chem. Rev. 109 (11) (2009) 5755–5798.

[4] D.E. Ingber, Mechanical signaling and the cellular response to extracellular matrix in angiogenesis and cardiovascular physiology, Circ. Res. 91 (10) (2002) 877–887.

[5] M.R. Louthan Jr., G.R. Caskey Jr., J.A. Donovan, D.E. Rawl Jr., Hydrogen embrittlement of metals, Mater. Sci. Eng. 10 (0) (1972) 357–368.

[6] Y. Liu, H. Zheng, X.H. Liu, S. Huang, T. Zhu, J. Wang, A. Kushima, N.S. Hudak, X. Huang, S. Zhang, S.X. Mao, X. Qian, J. Li, J.Y. Huang, Lithiation-induced embrittlement of multiwalled carbon nanotubes, ACS Nano 5 (9) (2011) 7245–7253.

[7] X. Huang, H. Yang, A.C.T. van Duin, K.J. Hsia, S. Zhang, Chemomechanics control of tearing paths in graphene, Phys. Rev. B 85 (19) (2012) 195453.

[8] M. ChrzanowskaWodnicka, K. Burridge, Rho-stimulated contractility drives the formation of stress fibers and focal adhesions, J. Cell Biol. 133 (6) (1996) 1403–1415.

[9] X.H. Liu, J.Y. Huang, In situ TEM electrochemistry of anode materials in lithium ion batteries, Energy Environ. Sci. 4 (10) (2011) 3844–3860.

[10] X.H. Liu, Y. Liu, A. Kushima, S. Zhang, T. Zhu, J. Li, J.Y. Huang, In situ TEM experiments of electrochemical lithiation and delithiation of individual nanostructures, Adv. Eng. Mater. 2 (7) (2012) 722–741.

[11] J.Y. Huang, L. Zhong, C.M. Wang, J.P. Sullivan, W. Xu, L.Q. Zhang, S.X. Mao, N.S. Hudak, X.H. Liu, A. Subramanian, H. Fan, L. Qi, A. Kushima, J. Li, In situ observation of the electrochemical lithiation of a single SnO_2 nanowire electrode, Science 330 (6010) (2010) 1515–1520.

[12] X.H. Liu, S. Huang, S.T. Picraux, J. Li, T. Zhu, J.Y. Huang, Reversible nanopore formation in Ge nanowires during lithiation–delithiation cycling: an in situ transmission electron microscopy study, Nano Lett. 11 (9) (2011) 3991–3997.

[13] X.H. Liu, H. Zheng, L. Zhong, S. Huang, K. Karki, L.Q. Zhang, Y. Liu, A. Kushima, W.T. Liang, J.W. Wang, J.-H. Cho, E. Epstein, S.A. Dayeh, S.T. Picraux, T. Zhu, J. Li, J.P. Sullivan, J. Cumings, C. Wang, S.X. Mao, Z.Z. Ye, S. Zhang, J.Y. Huang, Anisotropic swelling and fracture of silicon nanowires during lithiation, Nano Lett. 11 (8) (2011) 3312–3318.

[14] X.H. Liu, J.W. Wang, S. Huang, F. Fan, X. Huang, Y. Liu, S. Krylyuk, J. Yoo, S.A. Dayeh, A.V. Davydov, S.X. Mao, S.T. Picraux, S. Zhang, J. Li, T. Zhu, J.Y. Huang, In situ atomic-scale imaging of electrochemical lithiation in silicon, Nat. Nanotechnol. 7 (11) (2012) 749–756.

[15] X.H. Liu, L. Zhong, S. Huang, S.X. Mao, T. Zhu, J.Y. Huang, Size-dependent fracture of silicon nanoparticles during lithiation, ACS Nano 6 (2) (2012) 1522–1531.

[16] W. Liang, H. Yang, F. Fan, Y. Liu, X.H. Liu, J.Y. Huang, T. Zhu, S. Zhang, Tough germanium nanoparticles under electrochemical cycling, ACS Nano 7 (4) (2013) 3427–3433.

[17] H. Yang, S. Huang, X. Huang, F. Fan, W. Liang, X.H. Liu, L.-Q. Chen, J.Y. Huang, J. Li, T. Zhu, S. Zhang, Orientation-dependent interfacial mobility governs the anisotropic swelling in lithiated silicon nanowires, Nano Lett. 12 (4) (2012) 1953–1958.

[18] H. Yang, F. Fan, W. Liang, X. Guo, T. Zhu, S. Zhang, A chemo-mechanical model of lithiation in silicon, J. Mech. Phys. Solids 70 (0) (2014) 349–361.

[19] K.J. Zhao, M. Pharr, J.J. Vlassak, Z.G. Suo, Inelastic hosts as electrodes for high-capacity lithium-ion batteries, J. Appl. Phys. 109 (1) (2011) 016110.

[20] Y.F. Gao, M. Zhou, Strong stress-enhanced diffusion in amorphous lithium alloy nanowire electrodes, J. Appl. Phys. 109 (1) (2011).

[21] A.F. Bower, P.R. Guduru, A simple finite element model of diffusion, finite deformation, plasticity and fracture in lithium ion insertion electrode materials, Modelling Simul. Mater. Sci. Eng. 20 (4) (2012) 045004.

[22] S. Huang, F. Fan, J. Li, S. Zhang, T. Zhu, Stress generation during lithiation of high-capacity electrode particles in lithium ion batteries, Acta Mater. 61 (12) (2013) 4354–4364.

[23] R. Grantab, V.B. Shenoy, Pressure-gradient dependent diffusion and crack propagation in lithiated silicon nanowires, J. Electrochem. Soc. 159 (5) (2012) A584–A591.

[24] H. Yang, X. Huang, W. Liang, A.C.T. van Duin, M. Raju, S. Zhang, Self-weakening in lithiated graphene electrodes, Chem. Phys. Lett. 563 (0) (2013) 58–62.

[25] Z. Cui, F. Gao, J. Qu, Interface-reaction controlled diffusion in binary solids with applications to lithiation of silicon in lithium-ion batteries, J. Mech. Phys. Solids 61 (2) (2013) 293–310.

[26] X.H. Liu, F. Fan, H. Yang, S. Zhang, J.Y. Huang, T. Zhu, Self-limiting lithiation in silicon nanowires, ACS Nano 7 (2) (2012) 1495–1503.

[27] H. Haftbaradaran, H. Gao, W.A. Curtin, A surface locking instability for atomic intercalation into a solid electrode, Appl. Phys. Lett. 96 (9) (2010) 091909-3.

[28] M. Gu, H. Yang, D.E. Perea, J.-G. Zhang, S. Zhang, C.-M. Wang, Bending-induced symmetry breaking of lithiation in germanium nanowires, Nano Lett. 14 (8) (2014) 4622–4627.

[29] M.T. McDowell, S.W. Lee, J.T. Harris, B.A. Korgel, C. Wang, W.D. Nix, Y. Cui, In situ TEM of two-phase lithiation of amorphous silicon nanospheres, Nano Lett. 13 (2) (2013) 758–764.

[30] Y. Liu, X.H. Liu, B.-M. Nguyen, J. Yoo, J.P. Sullivan, S.T. Picraux, J.Y. Huang, S.A. Dayeh, Tailoring lithiation behavior by interface and bandgap engineering at the nanoscale, Nano Lett. 13 (10) (2013) 4876–4883.

[31] M.J. Chon, V.A. Sethuraman, A. McCormick, V. Srinivasan, P.R. Guduru, Real-time measurement of stress and damage evolution during initial lithiation of crystalline silicon, Phys. Rev. Lett. 107 (4) (2011) 045503.

[32] S.-P. Kim, D. Datta, V.B. Shenoy, Atomistic mechanisms of phase boundary evolution during initial lithiation of crystalline silicon, J. Phys. Chem. C 118 (31) (2014) 17247–17253.

[33] J.W. Wang, Y. He, F. Fan, X.H. Liu, S. Xia, Y. Liu, C.T. Harris, H. Li, J.Y. Huang, S.X. Mao, T. Zhu, Two-phase electrochemical lithiation in amorphous silicon, Nano Lett. 13 (2) (2013) 709–715.

[34] J.L. Goldman, B.R. Long, A.A. Gewirth, R.G. Nuzzo, Strain anisotropies and self-limiting capacities in single-crystalline 3D silicon microstructures: models for high energy density lithium-ion battery anodes, Adv. Funct. Mater. 21 (13) (2011) 2412–2422.

[35] S.W. Lee, M.T. McDowell, J.W. Choi, Y. Cui, Anomalous shape changes of silicon nanopillars by electrochemical lithiation, Nano Lett. 11 (7) (2011) 3034–3039.

[36] L.A. Berla, S.W. Lee, I. Ryu, Y. Cui, W.D. Nix, Robustness of amorphous silicon during the initial lithiation/delithiation cycle, J. Power Sources 258 (0) (2014) 253–259.

[37] M.T. McDowell, I. Ryu, S.W. Lee, C. Wang, W.D. Nix, Y. Cui, Studying the kinetics of crystalline silicon nanoparticle lithiation with in situ transmission electron microscopy, Adv. Mater. 24 (45) (2012) 6034–6041.